Article

# Conformational Dynamics Associated with Photodissociation of CO from Dehaloperoxidase Studied Using Photoacoustic Calorimetry

Jaroslava Miks#ovska#, Simona Horsa, Michael F. Davis, and Stefan Franzen

*Biochemistry*, **2008**, 47 (44), 11510-11517 • DOI: 10.1021/bi8012033 • Publication Date (Web): 10 October 2008



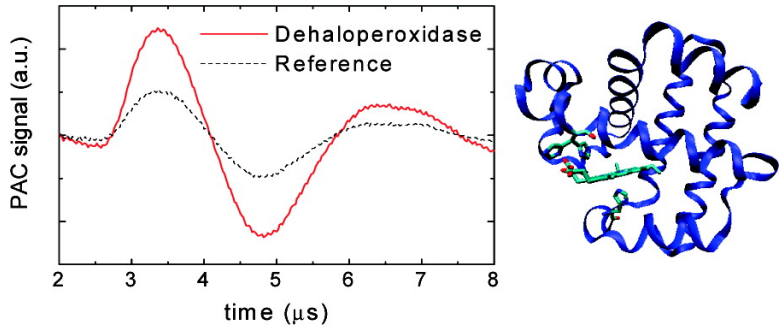


## More About This Article

Additional resources and features associated with this article are available within the HTML version:

- Supporting Information
- Access to high resolution figures
- Links to articles and content related to this article
- Copyright permission to reproduce figures and/or text from this article

View the Full Text HTML

# Conformational Dynamics Associated with Photodissociation of CO from Dehaloperoxidase Studied Using Photoacoustic Calorimetry[†]

Jaroslava Mikšovská,*[,‡] Simona Horsa,[‡] Michael F. Davis,[§] and Stefan Franzen[§]

*Department of Chemistry and Biochemistry, Florida International University, Miami, Florida 33199, and Department of Chemistry, North Carolina State University, Raleigh, North Carolina 27695*

*Received June 27, 2008; Revised Manuscript Received September 13, 2008*

ABSTRACT: Herein, we present photoacoustic calorimetry and transient absorption studies of the dynamics and energetics associated with dissociation of a ligand from $Fe^{2+}$ dehaloperoxidase (DHP) from *Amphitrite ornata*. Our data show that CO photodissociation is associated with an endothermic ($\Delta H = 8 \pm 3$ kcal mol$^{-1}$) volume expansion ($\Delta V = 9.4 \pm 0.6$ mL mol$^{-1}$) that occurs within 50 ns upon photodissociation. No additional thermodynamics were detected on slower time scales (up to 10 $\mu$s), suggesting that the dissociated ligand rapidly escapes from the heme-binding pocket into the surrounding solvent. Similar volume and enthalpy changes were observed for CO photodissociation in the presence of the substrate, 2,4-dichlorophenol or 4-bromophenol, indicating that either the substrate does not bind in the protein distal cavity at ambient temperature or its presence does not impact the thermodynamic profile associated with ligand dissociation. We attribute a fast ligand exchange between the protein active site and the surrounding solvent to the high flexibility of the distal histidine residue, His55, that provides a direct pathway between the heme-binding pocket and the protein exterior. The dynamics and energetics of conformational changes observed for dissociation of a ligand from DHP differ significantly from those measured previously for photodissociation of CO from the structural homologue myoglobin, suggesting that structural dynamics in DHP are fine-tuned to enhance the peroxidase function of this protein.

The mechanism associated with ligand binding to the active site of heme proteins has been extensively studied by time-resolved spectroscopic techniques in combination with site-directed mutagenesis and molecular dynamic simulations. In oxygen binding proteins, access of the ligand to the protein active site is modulated by large-scale fluctuations in protein structure that lead to the opening of transient pathways, allowing for ligand exchange between the heme-binding pocket and protein exterior (*1*−*4*). On the other hand, in peroxidases and catalases, a permanent access channel that links the enzyme active site cavity to aqueous exterior serves to facilitate delivery of substrate to the heme-binding pocket (*5, 6*). The hemoglobin dehaloperoxidase (DHP)[1] from the terebellid polychaete *Amphitrite ornata* (*7*−*10*) is an interesting example since it has a globin structure and peroxidase function. Enzymatic studies have indicated that DHP catalyzes $H_2O_2$-dependent dehalogenation of mono-, di-, or trihalophenols, and its catalytic activity is roughly intermediate between that of horseradish peroxidase (HRP) and myoglobin (Mb) (*11, 12*). Interestingly, native DHP can be isolated in the oxyferrous form (*13*), and the protein reversibly binds other diatomic ligands CO and NO (*14, 15*), suggesting that DHP may also serve as an oxygen binding and/or storage protein.

Structural studies have shown that DHP exhibits a high degree of sequence homology with intracellular globins from *Alvinella pompejana* (*16*) and its three-dimensional structure closely resembles that of Mb (*8*−*10, 17*). The prosthetic group, Fe protoporphyrin IX, is attached to the apoprotein through a coordination bond between the heme iron and the proximal residue His 89 (*10*). The proximal histidine lacks a strong hydrogen bond with a nearby aspartic acid residue that is characteristic of other peroxidases (*19*) and instead forms a weaker hydrogen bond to the carbonyl oxygen of nearby Leu 83 (*10*). Resonance Raman data show that the frequency of the Fe−N stretch is 233 cm$^{-1}$, significantly lower than that measured in other peroxidases with polarized histidine, indicating that His 89 is neutral and its electronic structure corresponds to that observed in other globins (*20*). In the ferric state, the heme iron is high-spin and six-coordinate with a water molecule situated ∼2.2 Å from the iron atom as shown by UV−vis (*14, 21*−*23*) and X-ray crystallography (*17*).

Unlike other peroxidases, DHP lacks a His-Arg pair in the heme distal pocket that facilitates cleavage of $H_2O_2$ (*19, 24*). The only polar residue located in the distal pocket of DHP is histidine, His 55. In the crystal structure determined by LaCount et al. (*10*), His 55 was found in two equally populated conformations, demonstrating an increased flexibility of its side chain at neutral pH (Figure 1). In the "closed" conformation, the imidazole side chain is situated

[†] This work was supported by the American Heart Association (Grant BGI 0665268B to J.M.).

* To whom correspondence should be addressed. Phone: (305) 348-7416. Fax: (305) 348-3772. E-mail: miksovsk@fiu.edu.

[‡] Florida International University.

[§] North Carolina State University.

[1] Abbreviations: 4-BP, 4-bromophenol; DHP, dehaloperoxidase; DCP, dichlorophenol; Fe(III)4SP, $Fe^{3+}$ tetrakis(4-sulfonatophenyl)porphine; HRP, horseradish peroxidase; Mb, myoglobin; PAC, photoacoustic calorimetry; TA, transient absorption.

10.1021/bi8012033 CCC: $40.75 
Published on Web 10/10/2008

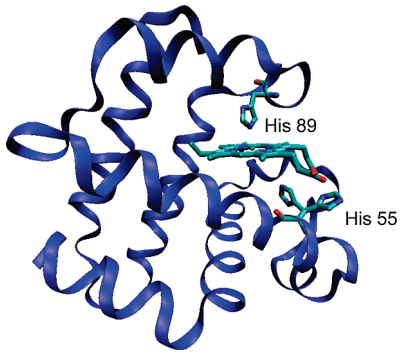


FIGURE 1: Structure of $Fe^{3+}$DHP (PBD entry 1EW6). Heme groups, as well as the proximal and distal His residues, are shown with a stick representation. His 55 is shown in the closed and open conformation.

within the distal pocket and the distance between the imidazole N$\varepsilon$2 atom and heme iron was reported to be ~5.5 Å, somewhat larger than in Mb. In the "open" position, the histidine side chain is rotated toward the external solution and its orientation strongly resembles that of His 64 in Mb at pH 4−4.5 (*25*). However, in more recently determined crystal structures of ferric and oxyferrous DHP resolved by Serrano et al. (*17*), His 55 was found only in the closed orientation with a distance between the N$\varepsilon$2 atom and heme iron of ~2.2 Å, suggesting that crystallization conditions may influence the position of the His 55 side chain. The conformational flexibility and substrate binding dynamics in DHP were investigated by Nienhaus et al. (*14*) using TDS FTIR spectroscopy and time-resolved absorption spectroscopy. Their results showed that CO-bound $Fe^{2+}$DHP adopts several conformations equivalent to those described previously for sperm whale Mb. At neutral pH, the major IR band was detected at 1950 $cm^{-1}$ and is associated with the closed conformation of His 55. At low pH, an additional IR band was found at 1965 $cm^{-1}$ and assigned to DHP in the open conformation with His 55 exposed to the surrounding solvent. It was also shown that the CO-bound $Fe^{2+}$DHP photoproduct exhibits a dominant band at 2127 $cm^{-1}$ that is analogous to the CO trapped in the primary docking B site in Mb (*14*).

The mode of substrate binding to DHP also remains rather controversial. On the basis of the crystal structure of DHP in a complex with the substrate analogue 2-iodophenol, it was proposed that organic substrates bind in the distal pocket and stabilize the open conformation with the proximal His 55 rotated out of the heme-binding pocket (*8*). Such penetration of the substrate molecule into the enzyme's active site is rather unusual for peroxidases, which interact with the substrate near the heme edge. However, recently published X-ray crystal structures show that binding of aromatic substrates at a partially internal site has been observed in ascorbate peroxidase (*26*). In the case of ascorbate peroxidase, such binding is likely involved in inhibition. By contrast, an internal substrate binding above the heme is observed in the cytochrome $P_{450}$ family of heme enzymes (*27*). FTIR, kinetics, and electron paramagnetic resonance experiments have confirmed that the substrate has effects in the distal pocket of DHP at cryogenic temperatures. The CO stretching frequency is shifted to 1972 $cm^{-1}$ at low pH when the substrate 2,4,6-trifluorophenol (TFP) is present. The CO recombination kinetics are substantially more rapid. EPR and hyperfine sublevel correlation spectroscopic (HYSCORE) analysis indicate that the water bound to the heme iron in the metaquo form of DHP is displaced when the substrate binds and the solution is frozen (*28*). However, studies have shown that TFP does not cause the CO frequency shift at room temperature in solution except at pH <5 (*29*). We have not yet found a method for proving that the substrate enters the heme pocket at room temperature under physiological conditions.

In this study, we use photoacoustic calorimetery (PAC) to probe the dynamics and energetics of structural changes associated with photodissociation of CO from $Fe^{2+}$DHP with and without bound substrate in terms of magnitudes and time profiles of molar volume and enthalpy changes. Although CO is not a physiological substrate for this enzyme, it is commonly used to investigate conformational dynamics coupled to ligand binding to other heme proteins due to the high quantum yield for photodissociation. In addition, the role of the substrate in modulating ligand access will also be examined using the substrates 2,4-dichlorophenol (2,4-DCP) and 4-bromophenol (4-BP), which are two of the most soluble substrates. Earlier photoacoustic calorimetry studies of photodissociation of CO from substrate free and camphore-bound cytochrome $P_{450}$ have shown that the conformational dynamics accompanying migration of the ligand out of the heme-binding pocket is strongly altered by the presence of substrate (*30*). Therefore, a detail description of the structural dynamics accompanying dissociation of a ligand from $Fe^{2+}$DHP will provide new insights into the mechanism of binding of substrate or cosubstrate to DHP and contribute to our understanding of factors that promote peroxidase activity in globular proteins.

## MATERIALS AND METHODS

2,4-Dichlorophenol (2,4-DCP) and 4-bromophenol (4-BP) were purchased from Sigma-Aldrich, and $Fe^{3+}$ tetrakis(4-sulfonatophenyl)porphine [Fe(III)4SP] was from Frontier-Scientific, Inc. Other chemicals were obtained from Fisher Scientific at the highest available purity.

*Protein Preparation.* Details of the recombinant protein expression, isolation, and purification are given elsewhere (*14*). DHP was dissolved in either 50 mM phosphate buffer (pH 7.0) or 50 mM acetate buffer (pH 4.0). Samples with bound substrate were prepared by dissolving DHP in either phosphate or acetate buffer containing 1 mM 2,4-DCP or 1 mM 4-BP. CO-bound $Fe^{2+}$DHP samples were obtained by placing samples into a 1 cm quartz cell sealed with a septum cap. The sample was then purged with Ar for approximately 30 min and reduced via addition of a few microliters of a freshly prepared 1 mM solution of sodium dithionite. Finally, the sample was saturated with CO. Formation of the $Fe^{2+}$- and CO-bound DHP adducts was verified by monitoring steady-state UV−vis spectra with a single-beam spectrophotometer (Cary 50, Varian). DHP concentrations were calculated using an $\varepsilon_{409}$ of 116 $mM^{-1}$ $cm^{-1}$ (*23*).

*Transient Absorption Spectroscopy.* The kinetics for CO rebinding and the quantum yields were determined using a transient absorption instrument of our own design (*31*). Samples were placed in a temperature-controlled cuvette holder (Quantum Northwest) and illuminated by the output of a 150 W Xe lamp focused on the center of the cuvette. The emerging light was then focused onto the entrance slit

of a monochromator (Micro HR, Jobin Yvon) and detected using a PMT (H6780, Spectra-Physics) coupled to a high-gain amplifier (70710, Spectra Physics). The signal was digitized using a 100 MHz transient digitizer (TDS 2012, Tektronix). Ligand dissociation was initiated by a 532 nm laser pulse (7 ns pulse width, 1 Hz repetition, 25 $\mu$J pulse power) from a frequency-doubled Nd:YAG laser (Minilite II, Continuum). Data were fitted by using a single-exponential decay function with Microcal Origin, version 5.0. The quantum yield for CO dissociation and bimolecular rebinding to $Fe^{2+}$DHP ($\Phi$) was determined using a laser photolysis method as described in ref *32* by employing CO-bound $Fe^{2+}$Mb as a reference:

$$\Phi = (\Delta A_{DHP}\Delta\varepsilon_{Mb}\Phi_{Mb})/(\Delta A_{Mb}\Delta\varepsilon_{DHP})$$

where $\Delta A$ is the initial absorbance change after ligand dissociation at 435 nm, $\Delta\varepsilon$ is the difference in the molar absorption coefficient between the CO-bound DHP and $Fe^{2+}$DHP at 435 nm obtained from the corresponding difference spectrum, $\Delta A_{Mb}$ is the initial absorbance change upon dissociation of CO from Mb at 435 nm, $\Delta\varepsilon_{Mb}$ is the difference in the molar absorption coefficient between the CO-bound and reduced Mb, and $\Phi_{Mb}$ is the quantum yield for the bimolecular photodissociation of CO from Mb that was previously determined to be 0.96 (*33*).

*Photoacoustic Spectroscopy.* The instrumentation for photoacoustic calorimetry and data analysis has been previously described in detail (*34, 35*). Briefly, the sample in the optical cell was placed in a temperature-controlled cuvette holder (Flash 200, Quantum Northwest), and a 1 MHz acoustic detector (TR-V103, Panametrics) was attached to the side of the cuvette. The coupling between the cuvette and the detector was facilitated by a thin layer of vacuum grease. The acoustic signal was amplified using a preamplifier (Panametrics 5662) and recorded with a 500 MHz digitizer (TDS 544A, Tektronix). CO photodissociation was initiated by the output from a frequency-doubled Nd:YAG laser (7 ns pulse, 1 Hz repetition rate, Minilite II, Continuum). The energy of the laser was kept below 50 $\mu$J to prevent multiphoton absorption. Typically, 30 traces were averaged to improve the signal-to-noise ratio.

The physical principle behind PAC is that a photoexcited molecule dissipates excess energy via vibrational relaxation to the surrounding solution. The prompt increase in temperature leads to a pressure wave resulting from a volume expansion that is detected by a pressure-sensitive detector. When the absorption of the laser pulse results in additional processes, such as dissociation of a covalent bond, electrostriction, etc., these processes also contribute to the overall volume change ($\Delta V$), which can be expressed as

$$\Delta V = \Delta V_{th} + \Delta V_{struct} \quad (1)$$

where $\Delta V_{th}$ represents the thermal volume change due to heat release (or heat uptake) to the solution. $\Delta V_{struct}$ includes volume changes other than those due to thermal heating, including volume changes due to protein conformational changes, electrostriction, etc. The thermal volume change can be written as

$$\Delta V_{th} = Q(\beta/C_p\rho) \quad (2)$$

where $Q$ is the amount of heat released to the solvent, $\beta$ is the coefficient of thermal expansion ($K^{-1}$), $C_p$ is the heat capacity (cal $g^{-1}$ $K^{-1}$), and $\rho$ is the density (g $mL^{-1}$). The amplitude of the acoustic signal for the sample can be then described as

$$S = E_aK[Q(\beta/C_p\rho) + \Delta V_{struct}] \quad (3)$$

where $E_a$ is the number of Einsteins absorbed by the sample and $K$ is the instrument's response constant. To eliminate $K$, the acoustic waves for the reference compound are measured under conditions identical to those used to obtain the sample traces. We have used Fe(III) 4SP as a reference compound, since it promptly converts the energy of the absorbed photon into heat with a quantum yield of unity. The amplitude of the acoustic wave for the reference compound is then described as

$$R = E_aKE_{h\nu}(\beta/C_p\rho) \quad (4)$$

where $E_{h\nu}$ is the energy of the photon at 532 nm. The ratio of the sample amplitude to the reference amplitude gives the following expression:

$$S/RE_{h\nu} = Q + \Delta V_{struct}(C_p\rho/\beta) \quad (5)$$

Thus, a plot of $S/RE_{h\nu}$ versus $C_p\rho/\beta$ leads to a linear relationship with a slope corresponding to $\Delta V_{struct}$ and an intercept equal to $Q$. For processes with a quantum yield ($\Phi$) of <1, the reaction enthalpy and volume changes are obtained using eqs 6 and 7, respectively.

$$\Delta H = (E_{h\nu} - Q)/\Phi \quad (6)$$

$$\Delta V = \Delta V_{struct}/\Phi \quad (7)$$

## RESULTS

The UV−vis spectrum of DHP at pH 7.0 exhibits a Soret band at 408 nm, low-intensity Q bands at 504 and 538 nm, and a weak charge transfer band at 635 nm. Upon heme reduction, the maximum of the Soret band shifts to 432 nm and a new band appears at 557 nm that is characteristic of a five-coordinate high-spin heme. The absorption spectrum of CO-bound $Fe^{2+}$DHP is similar to that of CO-bound $Fe^{2+}$ Mb with the Soret band maximum at 422 nm and $\alpha$ and $\beta$ bands located at 571 and 540 nm, respectively. The UV−vis spectrum of $Fe^{3+}$DHP measured at pH 4.0 shows an increase in the intensity of the Soret band and the appearance of a new band at 627 nm. These changes indicate partial destabilization of the protein structure at acidic pH. On the other hand, the absorption spectra of the reduced and CO-bound forms of DHP at pH 4.0 are very similar to those observed at pH 7.0, suggesting a greater stability of the reduced and CO-bound form of DHP toward pH-induced unfolding. Addition of 1 mM DCP or 4-BP to $Fe^{3+}$DHP at pH 7.0 results in an ~3 nm blue shift and a small decrease in the intensity of the Soret band. The spectra of $Fe^{2+}$DHP and CO-bound $Fe^{2+}$DHP in the presence of 1 mM 2,4-DCP or 1 mM 4-BP are nearly identical to those determined in the absence of substrate at both pH 7.0 and 4.0. Typical optical spectra of $Fe^{3+}$-, $Fe^{2+}$-, and CO-bound DHP at pH 4.0 and 1 mM 2,4-DCP are presented in Figure 2.

Volume and enthalpy changes associated with photodissociation of CO from $Fe^{2+}$DHP were measured using PAC. To probe the impact of the open and closed protein conformations on the structural dynamics in DHP, the data were collected at pH 4.0 and 7.0, respectively, since

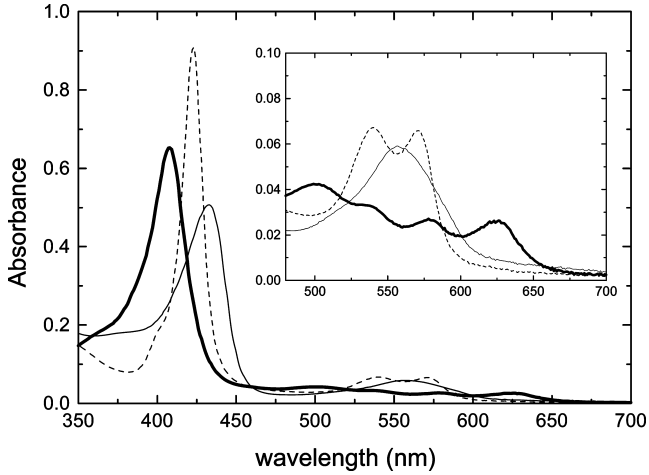


FIGURE 2: Steady-state UV−vis absorption spectra of $Fe^{3+}$DHP (thick solid line), $Fe^{2+}$DHP (thin solid line), and CO-bound DHP (dashed line) in acetate buffer (pH 4.0) and 1 mM 2,4-DCP.

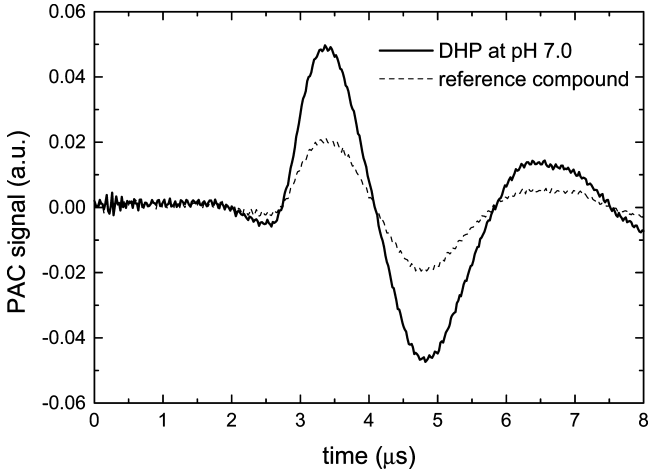


FIGURE 3: Overlay of acoustic traces for dissociation of CO from $Fe^{2+}$DHP and the reference compound, $Fe^{3+}$4SP. Conditions: 20 $\mu$M DHP in 50 mM phosphate buffer at pH 7.0 and 20 °C.

protonation of distal histidine at low pH is likely to stabilize it in the open conformation. Conformational flexibility of distal histidine was observed in the structure of $Fe^{3+}$DHP by Zhang et al. (*9, 10*) and recently by Chen et al. (*18*) for the deoxy form of DHP. To determine whether ionic interactions are involved in the conformational dynamics coupled to ligand photorelease, volume and enthalpy changes were also determined in solution at higher ionic strengths (500 mM NaCl). Finally, the influence of substrate binding on the structural dynamics in DHP was also examined. An overlay of sample and reference acoustic traces measured at 20 °C is presented in Figure 3 for dissociation of CO from $Fe^{2+}$DHP at pH 4.0 and 1 mM 2,4-DCP. The sample trace overlays in phase with the reference trace, indicating the absence of volume and enthalpy changes on time scales between ~50 ns and ~10 $\mu$s. The amplitude of the sample acoustic wave is approximately 2 times larger than the corresponding amplitude of the reference wave, demonstrating that ligand dissociation leads to distinct volume and enthalpy changes occurring within 50 ns. A plot of the ratio of sample and reference acoustic amplitudes as a function of $C_p\rho/\beta$ is shown in Figure 4. The reaction volume and enthalpy changes associated with dissociation of the ligand

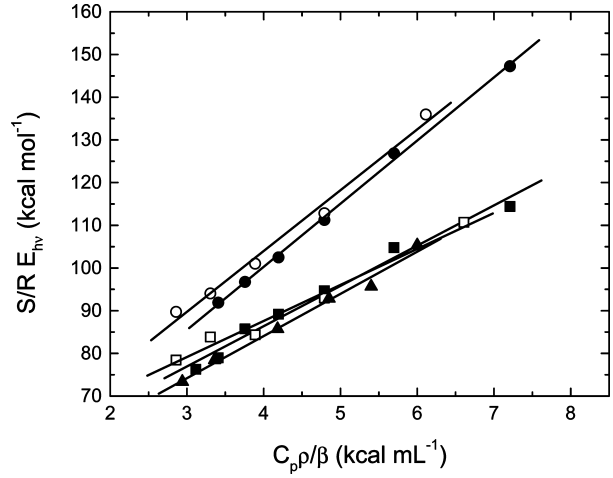


FIGURE 4: Plot of $(S/R)E_{h\nu}$ vs $C_p\rho/\beta$ for dissociation of CO from DHP in 50 mM phosphate buffer (pH 7.0) (squares), in 50 mM phosphate buffer (pH 7.0) and 1 mM 2,4-DCP, in 50 Tris buffer (pH 7.0) (circles), in 50 mM acetate buffer (pH 4.0), and in the presence of 2 mM dichlorophenol, 50 mM phosphate buffer (pH 7.4), and 500 mM NaCl.

from DHP were then extrapolated from the linear fits using eqs 5−7 and are listed in Table 1.

The reaction enthalpy change for photodissociation of CO from $Fe^{2+}$DHP ($\Delta H = 8 \pm 3$ kcal mol$^{-1}$ at pH 7.0, and $\Delta H = 13 \pm 2$ kcal mol$^{-1}$ at pH 4.0) can be described as $\Delta H = \Delta H_{str} + \Delta H_{Fe-CO}$, where $\Delta H_{str}$ represents the enthalpy change associated with protein structure relaxation and $\Delta H_{Fe-CO}$ is the enthalpy change for the Fe−CO bond cleavage and CO solvation upon entering the bulk solvent. Using a $\Delta H_{Fe-CO}$ of ~20 kcal mol$^{-1}$ (*34*), we estimate $\Delta H_{str}$ to be exothermic by approximately −12 kcal mol$^{-1}$ at pH 7.0 and approximately −7 kcal mol$^{-1}$ at pH 4.0. Similarly, the reaction volume change ($\Delta V$) can be expressed as $\Delta V = V_{CO} + V_{DHP} - V_{DHPCO}$, where $V_{DHP}$ is the partial molar volume of $Fe^{2+}$DHP and $V_{DHPCO}$ is the partial molar volume of CO-bound $Fe^{2+}$DHP. $V_{CO}$ represents the partial molar volume of CO reported previously to be 30 mL mol$^{-1}$ (*36*). From the observed $\Delta V$ of 9.4 ± 0.6 mL mol$^{-1}$ at neutral pH and 15.7 ± 0.7 mL mol$^{-1}$ at acidic pH, we estimate that the structural relaxation accompanying ligand dissociation ($\Delta V_{str} = V_{DHP} - V_{DHPCO}$) involves a volume decrease of approximately −21 mL mol$^{-1}$ at pH 7.0 and approximately −14 mL mol$^{-1}$ at pH 4.0. The data also show that the thermodynamic parameters measured in the presence of 1 mM substrate are very similar to those determined in the absence of substrate, pointing out that substrate binding to DHP does not alter the conformational dynamics in DHP upon ligand release. The observed volume and enthalpy changes are not sensitive to the ionic strength of the solution, indicating that electrostriction of solvent molecules does not contribute to the observed volume and enthalpy changes.

The quantum yields for CO photodissociation were determined using transient absorption spectroscopy as described in Materials and Methods and are listed in Table 2. Transient absorption traces for CO rebinding to $Fe^{2+}$DHP at 20 °C and 1 mM CO are presented in Figure 5. Traces were fit to a single-exponential decay model to determine the rate constant for CO rebinding. At pH 7.0, CO rebinds to $Fe^{2+}$DHP with a bimolecular rate constant of $1.3 \times 10^6$ M$^{-1}$ s$^{-1}$. The ligand rebinding is ~1.5 times faster at pH

Table 1: Volume and Enthalpy Changes Associated with Photodissociation of CO from DHP, HRP, and Horse Heart Mb

| | $\Delta V_1$ (mL mol$^{-1}$) | $\Delta H_1$ (kcal mol$^{-1}$) | $\Delta V_2$ (mL mol$^{-1}$) | $\Delta H_2$ (kcal mol$^{-1}$) |
|---|---|---|---|---|
| 50 mM phosphate (pH 7.0) | 9.4 ± 0.6 | 8 ± 3 | – | – |
| 50 mM phosphate (pH 7.4) and 500 mM NaCl | 9.9 ± 0.7 | 9 ± 3 | – | – |
| 50 mM phosphate (pH 7.0) and 1 mM 2,4-DCP | 8.4 ± 0.7 | 4 ± 3 | – | – |
| 50 mM phosphate (pH 7.0) and 1 mM 4-BP | 9.8 ± 1.6 | 11 ± 5 | | |
| 50 mM acetate (pH 4.0) | 15.7 ± 0.8 | 13 ± 2 | – | – |
| 50 mM acetate (pH 4.0) and 1 mM 2,4-DCP | 14 ± 1 | 7 ± 3 | – | |
| 50 mM acetate (pH 4) and 1 mM 4-BP | 11.8 ± 1.0 | 5 ± 5 | | |
| HRP[a] | 30 | 42 | – | – |
| horse heart myoglobin[b] | −2.5 ± 0.6 | 8 ± 3 | 14.3 ± 0.8 | 9 ± 4 |

[a] From ref *47*. [b] From ref *50*.

Table 2: Rate Constants for CO Rebinding to DHP and Quantum Yields for CO Photodissociation Determined Using Transient Absorption Spectroscopy

| | $k$ (M$^{-1}$ s$^{-1}$)[a] | $\Phi$[b] |
|---|---|---|
| phosphate buffer (pH 7.0) | $1.3 \times 10^6$ | 0.98 |
| phosphate buffer (pH 7.0) and 1 mM 2,4-DCP | $8.9 \times 10^5$ | 0.94 |
| acetate buffer (pH 4.0) | $1.9 \times 10^6$ | 0.98 |
| acetate buffer (pH 4.0) and 1 mM 2,4-DCP | $1.0 \times 10^6$ | 0.94 |

[a] Measured at 1 mM CO and 20 °C. [b] Error of ±0.05.

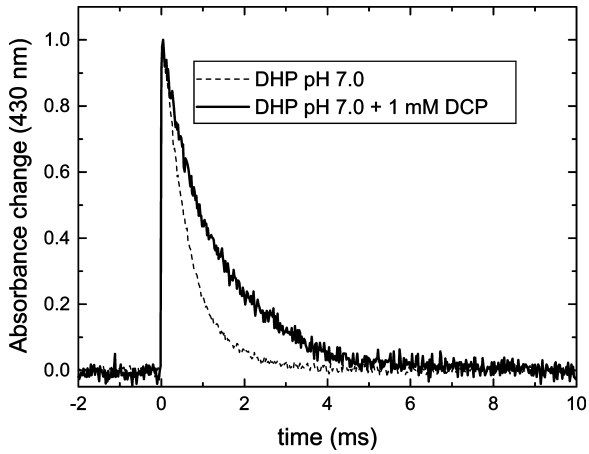


FIGURE 5: Transient absorption traces for CO rebinding to $Fe^{2+}$DHP. Conditions: 50 mM phosphate buffer (pH 7.0) (black solid line), 50 mM phosphate buffer (pH 7.0) and 1 mM 2,4-DCP (black dashed line), 50 mM acetate buffer (pH 4.0) (gray solid line), and 50 mM acetate buffer and 1 mM 2,4-DCP (gray dashed line).

4.0 ($k = 1.9 \times 10^6$ M$^{-1}$ s$^{-1}$) than at pH 7.0. The presence of 1 mM 2,4-DCP decreases the rate constant for CO rebinding ~1.5-fold at pH 7.0 and ~1.9-fold at pH 4.0. The measured rate constants are similar to those determined previously by Nienhaus et al. (*14*). These authors reported that CO rebinds to $Fe^{2+}$DHP with rate constants of $8.9 \times 10^5$ M$^{-1}$ s$^{-1}$ at pH 8.0 and $1.14 \times 10^6$ M$^{-1}$ s$^{-1}$ at pH 5.0. Considering that thermodynamic parameters for photodissociation of CO from DHP in the presence of 4-BP are similar to those determined in the presence of 2,4-DCP, the quantum yield for CO dissociation in the presence of 4-BP was not determined.

## DISCUSSION

Unlike time-resolved optical techniques, which are highly sensitive to the structural changes in the vicinity of a specific chromophore, photoacoustic calorimetry monitors the magnitudes and time profiles of overall volume and enthalpy changes and thus allows for the detection of conformational changes that are optically silent, i.e., do not directly affect the absorption spectrum of the chromophore molecule. Peters et al. (*37*−*39*) have initially employed PAC to study CO photodissociation from horse heart and sperm whale Mb. These studies were later expanded by Terazima's group (*40*−*42*) and Miller's group (*43*−*45*), who used transient grating techniques. It was shown that the cleavage of the Fe−CO bond results in a prompt ($\tau$ < 50 ns) volume decrease of roughly −3 mL mol$^{-1}$ and a positive enthalpy change of 8.0 kcal mol$^{-1}$. Subsequent ligand escape to surrounding solvent occurs with a lifetime of 700 ns at 20 °C and is accompanied by a volume increase of ~14 mL mol$^{-1}$ and an enthalpy change of 8.0 kcal mol$^{-1}$.

Despite a high degree of structural homology between Mb and DHP, the conformational dynamics associated with photodissociation of CO from $Fe^{2+}$DHP are distinct from those measured in Mb. At neutral pH, the cleavage of the Fe−CO bond leads to a prompt ($\tau$ < 50 ns) volume expansion of 9.4 ± 0.6 mL mol$^{-1}$ and an enthalpy change of 8 ± 3 kcal mol$^{-1}$. No additional volume and enthalpy changes were resolved on the time scale between ~50 ns and ~20 $\mu$s, indicating the absence of changes in protein conformation on this time scale. Structural changes located within the protein matrix may not lead to an observable change in volume, but the associated enthalpy change would be detected in photoacoustic measurements. Fragmentation reactions (e.g., bond cleavage reactions) lead to an increase in the amount of molecular surface exposed to the solvent and result in a volume increase due to perturbations in the packing of solvent molecules in the liquid (*46*). Thus, we attribute the observed positive volume and enthalpy changes to the dissociation of the Fe−CO bond and subsequent ligand escape into surrounding solvent. This is further confirmed by our preliminary photothermal beam deflection data that do not reveal any volume and enthalpy changes taking place on the microsecond to millisecond time scale (data not shown). The absence of conformational changes on nanosecond to microsecond traces is consistent with the lack of CO geminate recombination observed by flash photolysis at room temperature (*14*).

The results clearly indicate that escape of ligand to the surrounding solvent in DHP is more than 10 times faster than that in Mb. In Mb, the photodissociated ligand quickly migrates into internal Xe cavities, where it is trapped for hundreds of nanoseconds. Subsequent escape of ligand from the protein matrix occurs either through the distal His 64 gate or through transiently opened hydrophobic channels within the protein interior (*2*). Several factors may facilitate escape of ligand from the active site in DHP. The side chain of the distal His 55 was proposed to be flexible on the basis of the crystal structure of $Fe^{3+}$DHP determined by Lebioda et al. (*8, 10*). This was further confirmed by a recent structure

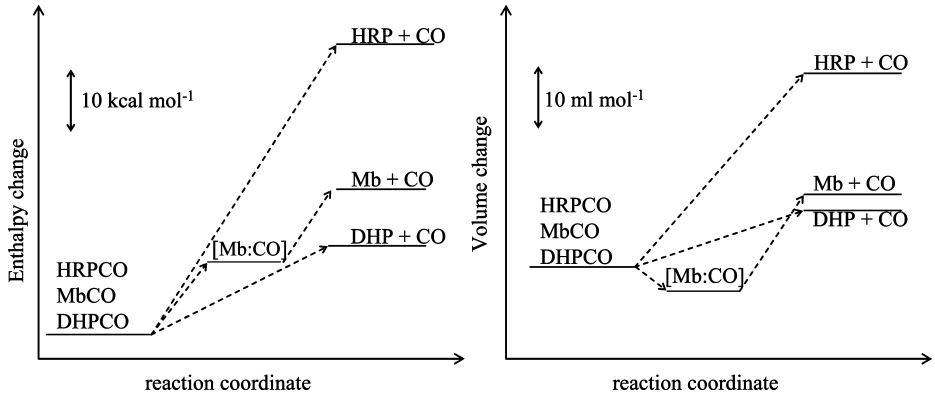


FIGURE 6: Enthalpy and volume profiles for dissociation of CO from DHP, horse heart Mb, and HRP. In the case of HRP and DHP, CO migrates out of the protein matrix within 50 ns, whereas in Mb, the ligand photodissociation results in the formation of an intermediate with CO located in the distal pocket ([Mb:CO]) and subsequent CO release to the solution occurs on the 700 ns time scale.

of $Fe^{2+}$DHP in which His 55 was found in three distinct conformations (*18*). Two open conformations correspond to the imidazole side chain in the solvent-exposed orientation (39 and 17% occupancy), whereas the third conformation corresponds to the histidine side chain located within the distal pocket (44% occupancy). In the solvent-exposed conformation, the imidazole side chain is displaced from the heme-binding site, which results in the opening of a direct channel connecting the heme pocket with aqueous solvent that may be used for fast ligand escape. Unlike Mb, there is no water molecule in the distal pocket of the deoxy form. This observation suggests that there is no exchange of CO and $H_2O$ in the escape process and hence a smaller barrier to CO escape than in photolyzed MbCO. In addition, the fast escape of CO from $Fe^{2+}$DHP as measured by PAC indicates that the photodissociated ligand does not migrate into protein internal cavities. As a consequence, there is no trapping of the CO in the protein interior on the submicrosecond time scale and essentially no geminate recombination to the heme iron. This is also evident from the results of TDS FTIR spectroscopy (*14*). Nienhaus et al. reported that in DHP only 10% of the photodissociated ligand migrates from the primary docking site into the protein interior at 80 K. The low yield for the photodissociated ligand in the secondary docking site was attributed to the fact that amino acid residues analogous to those that define hydrophobic cavities in the Mb structure are to some extent reoriented in the DHP structure, resulting in decreased access to secondary CO binding sites. Interestingly, the observed fast escape of ligand from the DHP active site is consistent with the photoacoustic data on photorelease of CO from HRP showing that in this enzyme the dissociated ligand migrates into the surrounding solvent within the first 20 ns upon dissociation (*47*). These data show that although trapping of diatomic ligands in the protein matrix is important for the function of Mb and other oxygen storage proteins (*2*), this feature is not preserved in DHP. In fact, accumulation of peroxide in the vicinity of the DHP active site is likely to lead to a progressive enzyme inactivation.

The measured thermodynamic parameters further demonstrate that at pH 7.0 the conformational relaxation associated with ligand photorelease is exothermic ($\Delta H = -12$ kcal $mol^{-1}$) and exhibits a volume decrease of $-21$ mL $mol^{-1}$. The molecular origin of the observed volume and enthalpy changes remains ambiguous. One contribution that is present in all myoglobins and hemoglobins is the doming of the porphyrin ring due to the low-spin six-coordinate to high-spin five-coordinate heme iron transition and the accompanying relaxation of the proximal histidine, His 89 in DHP. The changes on the distal side are pH-dependent and appear to dominate the photoacoustic response. The recently obtained high-resolution X-ray structure of $Fe^{2+}$DHP and $O_2$-bound mutant $Fe^{2+}$DHP at pH 6 (having Cys 73 replaced with Ser; PDB entries 2QFK and 2QFN, respectively) (*17*) shows that hydrogen bonding between H55 and $O_2$ is strong at ~100 K, which correlates with 100% occupancy of H55 in the distal pocket. In the deoxy form, H55 is largely in a solvent-exposed (open) conformation or shows disorder in the distal pocket at the same pH (*18*). Thus, binding of $O_2$ causes His 55 to enter the distal pocket and reorient in such a way that N$\delta$1 is exposed to the solvent and N$\varepsilon$2 forms a strong hydrogen bond with the second oxygen atom. We expect that the His 55 side chain adopts a similar orientation in both $O_2$- and CO-bound complexes of $Fe^{2+}$DHP since the FTIR data demonstrate that His 55 forms a hydrogen bond with the ligand oxygen in CO-bound $Fe^{2+}$DHP (*14*). In such a case, the volume and enthalpy changes associated with the structural relaxation at pH 7.0 can be attributed to reorientation of His 55 and alteration of the hydrogen bonding network in the distal pocket. The acoustic data also show that the conformational relaxation at pH 4.0 is less exothermic and exhibits less volume contraction than at pH 7.0. At acidic pHs, an increased fraction of DHP is in the open conformation with the His 55 side chain rotated out of the distal pocket as shown by UV−vis titration data and FTIR studies (*14*). Therefore, the difference between the volume and enthalpy changes observed at pH 7.0 and 4.0 reflects His 55 reorientation and subsequent reorganization of the hydrogen bond network which takes place at pH 7.0 but appears to be absent at pH 4.0.

Interestingly, the reaction volume and enthalpy changes for dissociation of CO from DHP at pH 7.0 do not match the overall enthalpy change ($\Delta H_1 + \Delta H_2$) and volume change ($\Delta V_1 + \Delta V_2$) observed for photorelease of CO from the structural analogue Mb or those observed for dissociation of CO from the functional analogue HRP (Table 1 and Figure 6), suggesting differences in the magnitude of protein relaxations in those proteins subsequent to ligand release. Feis and Angeloni (*47*) have proposed that photorelease of ligand from HRP is not associated with substantial changes in protein conformation and that the measured volume and enthalpy changes reflect solvation of the CO molecule and

dissociation of the Fe−CO bond, respectively. In myoglobin, the out-of-plane displacement of the heme iron due to ligand dissociation leads to an overall conformational relaxation, including a scissor-like motion of the E and F helices (*48*). Structural changes within the porphyrin ring were proposed to be transmitted into the protein matrix via the proximal His 93, which is located near the end of the F helix (*4*). In DHP, the α-helix that corresponds to the F helix in Mb is one turn shorter, which places the proximal His 89 in an unstructured loop located between two α-helices. This conformation leads to increased flexibility of the proximal histidine in DHP. Therefore, the structural changes associated with the porphyrin ring may not lead to the same structural relaxation that occurs in Mb upon ligand release.

## CONCLUSION

We have investigated the impact of substrate binding on the conformational dynamics associated with photodissociation of CO from $Fe^{2+}$DHP. The binding of 4-iodophenol in the distal pocket of DHP observed in the room-temperature X-ray crystal structure (*10*) suggested initially that there would be large effects of substrate binding on the photoacoustic response of photolyzed CO. However, the volume changes associated with photodissociation of CO from DHP in the presence of 1 mM 2,4-DCP closely resemble those detected in the absence of substrate, and the enthalpy changes are only slightly smaller at both neutral and acidic pH. These data are consistent with recent $^1$H hyperfine NMR results that show that 2,4-DCP and 4-BP bind dynamically in the distal pocket of six-coordinate cyanide-bound DHP and 2,4,6-TFP binds on the surface (*49*). The lack of an effect of any of these substrates on the photoacoustic signal suggests, therefore, that binding of these substrates to CO-bound $Fe^{2+}$DHP does not result in a thermodynamic/kinetic barrier to migration of ligand to the bulk solvent. This conclusion is further confirmed by the results of our transient absorption study that show similar quantum yields and bimolecular rate constants for CO rebinding to $Fe^{2+}$DHP in the presence and absence of 2,4-DCP. Substrate binding in the distal pocket would be expected to significantly decrease the volume of the distal pocket, which would affect both the quantum yield and rates for CO rebinding. The hypothesis that ligand escape dominates the photoaccoustic signal is consistent with a recent X-ray crystal structure that shows a high flexibility of the distal histidine, H55 in the deoxy form (*18*). Thus, we can conclude that even under conditions (such as low pH) where the substrate binds in the distal pocket, the CO ligand can easily escape because of the combination of the flexibility of the distal histidine, H55, and steric blocking of secondary binding sites in the distal pocket. The ease of ligand escape, the negative change in volume, and the lack of a strong substrate effect demonstrated in the photoacoustic and transient absorption data are key observations that confirm the uniqueness of the DHP distal pocket in the hemoglobin family.

## REFERENCES


1. Ostermann, A., Waschipky, R., Parak, F. G., and Nienhaus, G. U. (2000) Ligand binding and conformational motions in myoglobin. *Nature 404*, 205–208.
2. Scott, E. E., Gibson, Q. H., and Olson, J. S. (2001) Mapping of pathways for $O_2$ entry into and exit from myoglobin. *J. Biol. Chem. 276*, 5177–5188.
3. Brunori, M. (2000) Structural dynamics of myoglobin. *Biophys. Chem. 86*, 221–230.
4. Perutz, M. F. (1979) Regulation of oxygen affinity of hemoglobin: Influence of structure of the globin on the heme iron. *Annu. Rev. Biochem. 48*, 327–386.
5. Khajehpour, M., Rietveld, I., Vinogradov, S., Prabhu, N. V., Sharp, K. A., and Vanderkooi, J. M. (2003) Accessibility of oxygen with respect to the heme pocket in horseradish peroxidase. *Proteins 53*, 656–666.
6. Chelikani, P., Carpena, X., Fita, I., and Loewen, P. C. (2003) An Electrical Potential in the Access Channel of Catalases Enhances Catalysis. *J. Biol. Chem. 278*, 31290–31296.
7. Chen, Y. P., Woodin, S. A., Lincoln, D. E., and Lovell, C. R. (1996) An unusual dehalogenating peroxidase from the marine terebellid polychaete *Amphitrite ornata*. *J. Biol. Chem. 271*, 4609–4612.
8. Lebioda, L., LaCount, M. W., Zhang, E., Chen, Y. P., Han, K., Whitton, M. M., Lincoln, D. E., and Woodin, S. A. (1999) An enzymatic globin from a marine worm. *Nature 401*, 445.
9. Zhang, E., Chen, Y. P., Roach, M. P., Lincoln, D. E., Lovell, C. R., Woodin, S. A., Dawson, J. H., and Lebioda, L. (1996) Crystallization and initial spectroscopic characterization of the heme-containing dehaloperoxidase from the marine polychaete *Amphitrite ornata*. *Acta Crystallogr. D52*, 1191–1193.
10. LaCount, M. W., Zhang, E., Chen, Y. P., Han, K., Whitton, M. M., Lincoln, D. E., Woodin, S. A., and Lebioda, L. (2000) The crystal structure and amino acid sequence of dehaloperoxidase from *Amphitrite ornata* indicate common ancestry with globins. *J. Biol. Chem. 275*, 18712–18716.
11. Belyea, J., Gilvey, L. B., Davis, M. F., Godek, M., Sit, T. L., Lommel, S. A., and Franzen, S. (2005) Enzyme function of the globin dehaloperoxidase from *Amphitrite ornata* is activated by substrate binding. *Biochemistry 44*, 15637–15644.
12. Osborne, R. L., Taylor, L. O., Han, K. P., Ely, B., and Dawson, J. H. (2004) *Amphitrite ornata* dehaloperoxidase: Enhanced activity for the catalytically active globin using MCPBA. *Biochem. Biophys. Res. Commun. 324*, 1194–1198.
13. Zhang, E., Chen, Y. P., Roach, M. P., Lincoln, D. E., Lovell, C. R., Woodin, S. A., Dawson, J. H., and Lebioda, L. (1996) Crystallization and initial spectroscopic characterization of the heme-containing dehaloperoxidase from the marine polychaete *Amphitrite ornate*. *Acta Crystallogr. D52*, 1191–1193.
14. Nienhaus, K., Deng, P. C., Belyea, J., Franzen, S., and Nienhaus, G. U. (2006) Spectroscopic study of substrate binding to the carbonmonoxy form of dehaloperoxidase from *Amphitrite ornata*. *J. Phys. Chem. B 110*, 13264–13276.
15. Franzen, S., Jasaitis, A., Belyea, J., Brewer, S. H., Casey, R., MacFarlane, A. W., IV, Stanley, R. J., Vos, M. H., and Martin, J. L. (2006) Hydrophobic distal pocket affects NO-heme geminate recombination dynamics in dehaloperoxidase and H64V myoglobin. *J. Phys. Chem. B 110*, 14483–14493.
16. Bailly, X., Chabasse, C., Hourdez, S., Dewilde, S., Martial, S., Moens, L., and Zal, F. (2007) Globin gene family evolution and functional diversification in annelids. *FEBS J. 274*, 2641–2652.
17. deSerrano, V., Chen, Z., Davis, M. F., and Franzen, S. (2007) X-ray crystal structural analysis of the binding site in the ferric and oxyferrous forms of the recombinant heme dehaloperoxidase cloned from *Amphitrite ornata*. *Acta Crystallogr. D63*, 1094–1101.
18. Chen, Z., deSerrano, V., Betts, L., and Franzen, S. (2008) Increased distal histidine conformational flexibility in the deoxy form of dehaloperoxidase from *Amphitrite ornata*. *Acta Crystallogr.* (in press).
19. Finzel, B. C., Poulos, T. L., and Kraut, J. (1984) Crystal structure of yeast cytochrome c peroxidase refined at 1.7-Å resolution. *J. Biol. Chem. 259*, 13027–13036.
20. Franzen, S., Roach, M. P., Chen, Y. P., Dyer, R. B., Woodruff, W. H., and Dawson, J. H. (1998) The unusual reactivities of *Amphitrite ornata* dehaloperoxidase and *Notomastus lobatus* chloroperoxidase do not arise from a histidine imidazolate proximal heme iron ligand. *J. Am. Chem. Soc. 120*, 4658–4661.
21. Belyea, J., Belyea, C. M., Lappi, S., and Franzen, S. (2006) Resonance Raman study of ferric heme adducts of dehaloperoxidase from *Amphitrite ornata*. *Biochemistry 45*, 14275–14284.
22. Roach, M. P., Chen, Y. P., Woodin, S. A., Lincoln, D. E., Lovell, C. R., and Dawson, J. H. (1997) *Notomastus lobatus* chloroperoxidase and *Amphitrite ornata* dehaloperoxidase both contain histidine as their proximal iron ligand. *Biochemistry 36*, 2197–2202.
23. Osborne, R. L., Sumithran, S., Coggins, M. K., Chen, Y. P., Lincoln, D. E., and Dawson, J. H. (2006) Spectroscopic charac-

terization of the ferric states of *Amphitrite ornata* dehaloperoxidase and *Notomastus lobatus* chloroperoxidase: His-ligated peroxidases with globin-like proximal and distal properties. *J. Inorg. Biochem. 100*, 1100–1108.
24. Poulos, T. L., and Kraut, J. (1980) The stereochemistry of peroxidase catalysis. *J. Biol. Chem. 225*, 8199–8205.
25. Yang, F., and Phillips, G. N., Jr. (1996) Crystal structures of CO-, deoxy- and met-myoglobins at various pH values. *J. Mol. Biol. 256*, 762–774.
26. Sharp, K. H., Moody, P. C. E., Brown, K. A., and Raven, E. L. (2004) Crystal structure of ascorbate peroxidase-salicylhydroxamic acid complex. *Biochemistry 43*, 8644–8651.
27. Poulos, T. L., Finzel, B. C., and Howard, A. J. (1987) High resolution crystal structure of cytochrome P450 cam. *J. Mol. Biol. 195*, 687–700.
28. Smirnova, T. I., Weber, R. T., Davis, M. F., and Franzen, S. (2008) Substrate binding triggers a switch in the iron coordination in dehaloperoxidase from *Amphitrite ornata*: HYSCORE experiments. *J. Am. Chem. Soc. 130*, 2128–2129.
29. Nienhaus, K., Nickel, E., Davis, M. F., Franzen, S., and Nienhaus, G. U. (2008) Determinants of substrate internalization in distal pocket of dehaloperoxidse hemoglobin of *Amphitrite ornate*. *Biochemistry* (in press).
30. Di Primo, C., Deprez, E., Sligar, S. G., and Hui Bon Hoa, G. (1997) Origin of the photoacoustic signal in cytochrome P-450cam: Role of the Arg186-Asp251-Lys178 bifurcated salt bridge. *Biochemistry 36*, 112–118.
31. Miksovska, J., Yom, J., Diamond, B., and Larsen, R. W. (2006) Spectroscopic and photothermal study of myoglobin conformational changes in the presence of sodium dodecyl sulfate. *Biomacromolecules 7*, 476–482.
32. Hoshino, M., Ozawa, K., Seki, H., and Ford, P. C. (1993) Photochemistry of nitric oxide adducts of water-soluble iron(III) porphyrin and ferrihemoproteins studied by nanosecond laser photolysis. *J. Am. Chem. Soc. 115*, 9568–9575.
33. Henry, E. R., Sommer, J. H., Hofrichter, J., and Eaton, W. A. (1983) Geminate recombination of carbon monoxide to myoglobin. *J. Mol. Biol. 166*, 443–451.
34. Larsen, R. W., and Miksovska, J. (2007) Time resolved thermodynamics of ligand binding to heme proteins. *Coord. Chem. Rev. 251*, 1045–1310.
35. Gensch, T., and Viappiani, C. (2003) Time-resolved photothermal methods: Accessing time-resolved thermodynamics of photoinduced processes in chemistry and biology. *Photochem. Photobiol. Sci. 2*, 699–721.
36. Eley, D. D. (1939) On the solubility of gases. Part II. A comparison of organic solvents with water. *Trans. Faraday Soc. 35*, 1421.
37. Westrick, J. A., Goodman, J. L., and Peters, K. S. (1987) A time-resolved photoacoustic calorimetry study of the dynamics of enthalpy and volume changes produced in the photodissociation of carbon monoxide from sperm whale carboxymyoglobin. *Biochemistry 26*, 8313–8318.
38. Westrick, J. A., Peters, K. S., Ropp, J. D., and Sligar, S. G. (1990) Role of the arginine-45 salt bridge in ligand dissociation from sperm whale carboxymyoglobin as probed by photoacoustic calorimetry. *Biochemistry 29*, 6741–6746.
39. Westrick, J. A., and Peters, K. S. (1990) A photoacoustic calorimetric study of horse myoglobin. *Biophys. Chem. 37*, 73–79.
40. Sakakura, M., Yamaguchi, S., Hirota, N., and Terazima, M. (2001) Dynamics of structure and energy of horse carboxymyoglobin after photodissociation of carbon monoxide. *J. Am. Chem. Soc. 123*, 4286–4294.
41. Sakakura, M., Morishima, I., and Terazima, M. (2002) Structural dynamics of distal histidine replaced mutants of myoglobin accompanied with the photodissociation reaction of the ligand. *Biochemistry 41*, 4837–4846.
42. Nishihara, Y., Sakakura, M., Kimura, Y., and Terazima, M. (2004) The escape process of carbon monoxide from myoglobin to solution at physiological temperature. *J. Am. Chem. Soc. 126*, 11877–11888.
43. Dadusc, G., Ogilvie, J. P., Schulenberg, P., Marvet, U., and Miller, R. J. D. (2001) Diffractive optics-based heterodyne-detected four-wave mixing signals of protein motion: From "protein quakes" to ligand escape for myoglobin. *Proc. Natl. Acad. Sci. U.S.A. 98*, 6110–6115.
44. Walther, M., Raicu, V., Ogilvie, J. P., Phillips, R., Kluger, R., and Miller, R. J. D. (2005) Determination of the Fe-CO bond energy in myoglobin using heterodyne-detected transient thermal phase grating spectroscopy. *J. Phys. Chem. B 109*, 20605–20611.
45. Deak, J., Chiu, H.-L., Lewis, C. M., and Miller, R. J. D. (1998) Ultrafast phase grating studies of heme proteins: Observation of the low-frequency modes directing functionally important protein motions. *J. Phys. Chem. B 102*, 6621–6634.
46. Schmidt, R., and Schutz, M. (1996) Determination of reaction volumes and reaction enthalpies by photoacoustic calorimetry. *Chem. Phys. Lett. 263*, 795–802.
47. Feis, A., and Angeloni, L. (2001) Phododissociation of the CO complex of horseradish peroxidase studied by laser-induced optoacoustic spectroscopy. *J. Phys. Chem. 105*, 2638.
48. Vojtechovksy, J., Chu, K., Berendzen, J., Sweet, R. M., and Schlichting, I. (1999) Crystal structure of myoglobin-ligand complexes at near atomic resolution. *Biophys. J. 77*, 2153–2174.
49. Davis, M. F., Gracz, H., Vendeix, F. A. P., Gilvey, L. B., Somasundaram, A., Decatour, S. M., and Franzen, S. (2008) Different binding modes of mono-, di-, and trihalogenated phenols to the hemoglobin dehaloperoxidase from *Amphitrite ornate*. *Biochemistry* (in press).
50. Belogortseva, N., Rubio, M., Terrell, W., and Miksovska, J. (2007) The contribution of heme propionate groups to the conformational dynamics associated with CO photodissociation from horse heart myoglobin. *J. Inorg. Biochem. 101*, 977–986.

BI8012033